BBA - Biomembranes 1859 (2017) 2155–2160

Contents lists available at ScienceDirect

BBA - Biomembranes

journal homepage: www.elsevier.com/locate/bbamem

Solubilization of human cells by the styrene–maleic acid copolymer: Insights from fluorescence microscopy

Jonas M. Dörr[a,*], Marleen H. van Coevorden-Hameete[b], Casper C. Hoogenraad[b], J. Antoinette Killian[a,*]

[a] Membrane Biochemistry and Biophysics, Bijvoet Center for Biomolecular Research, Institute of Biomembranes, Utrecht University, Padualaan 8, 3584 CH Utrecht, The Netherlands
[b] Cell Biology, Department of Biology, Faculty of Science, Utrecht University, Padualaan 8, 3584 CH Utrecht, The Netherlands

ARTICLE INFO

Keywords:
Native nanodiscs
SMA-resistant membranes
Preferential solubilization
Cellular localization
Plasma membrane organization
Membrane domain

ABSTRACT

Extracting membrane proteins from biological membranes by styrene–maleic acid copolymers (SMAs) in the form of nanodiscs has developed into a powerful tool in membrane research. However, the mode of action of membrane (protein) solubilization in a cellular context is still poorly understood and potential specificity for cellular compartments has not been investigated. Here, we use fluorescence microscopy to visualize the process of SMA solubilization of human cells, exemplified by the immortalized human HeLa cell line. Using fluorescent protein fusion constructs that mark distinct subcellular compartments, we found that SMA solubilizes membranes in a concentration-dependent multi-stage process. While all major intracellular compartments were affected without a strong preference, plasma membrane solubilization was found to be generally slower than the solubilization of organelle membranes. Interestingly, some plasma membrane-localized proteins were more resistant against solubilization than others, which might be explained by their presence in specific membrane domains with differing properties. Our results support the general applicability of SMA for the isolation of membrane proteins from different types of (sub)cellular membranes.

1. Introduction

In recent years, styrene–maleic acid (SMA) copolymers have rapidly gained attention for applications in membrane research [1,2]. These include the detergent-free extraction and purification of integral membrane proteins from a variety of expression systems [3–5] and the study of lipid–protein interactions in the resulting native nanodiscs [5,6]. Importantly, these SMA-bounded nanodiscs generally mediate a higher protein stability than detergent micelles [3–5], which makes SMA extraction a promising alternative to established detergent-based methods.

Approaches involving lipid model membrane systems have contributed vastly to our understanding of the mode of action of membrane solubilization by SMA and the physico-chemical properties of the resulting SMA–lipid particles (SMALPs) [7–13]. However, systematic studies addressing the solubilization of (sub)cellular membranes by SMA are not available to date. These are important since the membranes of living cells are far more complex in composition and organization than are common lipid model membranes [14], with a substantial mass fraction being constituted by protein. These differing properties of biomembranes may have major consequences for their solubilization by SMA, especially if membrane proteins are isolated from more complex cells that contain subcellular compartments.

In this study, we employed HeLa cells to study the process of membrane solubilization by SMA in a cellular context. HeLa cells were selected because (i) they are the most commonly used human cell line, (ii) they are relatively easy to culture and general protocols for transfection with various DNA constructs are available and (iii) they exhibit strong adhesion to surfaces, which is beneficial for in-plane microscopy in the presence of solubilizing agent. In particular, we investigated whether SMA solubilization of membrane proteins depends on their localization in different (sub)cellular membranes. To this end, we used a variety of fluorescent membrane protein fusion constructs targeted to the membranes of different organelles or to the plasma membrane and followed their solubilization by multi-channel fluorescence microscopy. In addition, water-soluble fluorescent proteins with differing cellular localizations were used to assess membrane perforation. The results provide insights into the solubilization of membranes by SMA in a

Abbreviations: SMA, styrene–maleic acid; MARCKS, C-terminal truncation of myristoylated alanine-rich C-kinase substrate

* Corresponding authors.
E-mail addresses: j.m.dorr@uu.nl (J.M. Dörr), j.a.killian@uu.nl (J.A. Killian).

http://dx.doi.org/10.1016/j.bbamem.2017.08.010
Received 31 March 2017; Received in revised form 8 August 2017; Accepted 13 August 2017
Available online 25 August 2017

standard human cell line and into the susceptibility of different types of membranes in this process.

2. Material & methods

2.1. Materials

Xiran30010, a styrene–maleic anhydride polymer with a molar ratio of styrene to maleic anhydride monomer units of 2:1 and a weight-average molecular weight of 10 kDa, was a kind gift from Polyscope (Geleen, The Netherlands). Conversion to the acid form by hydrolysis and preparation of stock solutions at 5% (w/v) was performed as described elsewhere [8]. Hoechst 33342 (NucBlue® Live ReadyProbes® Reagent solution) was from Thermo Fisher Scientific (Waltham, MA), polyethylenimine PEI MAX was from Polysciences (Warrington, PA), Triton X-100 and all other chemicals were purchased from Sigma Aldrich (St. Louis, MO).

2.2. DNA constructs

All DNA constructs used have been described before. Constructs encoding for soluble proteins include tagRFP-ER (Molecular Probes, Eugene, OR) that contains an N-terminal calreticulin signal sequence and a C-terminal KDEL sequence resulting in localization to the ER lumen, MitoDsRed [15], encoding for the mitochondrial targeting sequence derived from the precursor of subunit VIII of human cytochrome C oxidase and a pEGFP N1 vector for marking the cytosol with GFP. Constructs encoding for membrane proteins were MARCKS-GFP and MARCKS-RPF (MARCKS–TagRFP-T) [16], both encoding for a truncated version of human myristoylated alanine-rich C-kinase substrate (MARCKS), comprising the 41 N-terminal amino acids in which Ala3 was mutated into Cys to introduce a palmitoylation site, TOM20-mCherry (TOM20-mCherry-LOVpep) [17], encoding for human mitochondrial import receptor TOM20 homolog, located in the outer mitochondrial membrane, CD8-ΔC-GFP [18], encoding for a truncated version of cluster of differentiation 8 that in T cells is plasma membrane localized but is not exported out of the ER in HeLa cells. Man II-GFP [19], encoding for the Golgi-resident human mannosidase 2 was a gift from John Presley, McGill University and NGL3-EGFP [20], encoding for rat Netrin-G ligand 3, a plasma membrane-localized protein was a gift from Eunjoon Kim, KAIST.

2.3. Sample preparation and fluorescence microscopy

HeLa cells were cultured in a 1:1 mixture of DMEM and Ham's F10 medium (Lonza, Basel Switzerland), containing 10% Fetal Calf Serum and 1% penicillin/streptomycin. Before splitting, cells were detached using trypsin/EDTA. For microscopy, cells were seeded on glass coverslips and transfection was performed using polyethylenimine. After transfection, cells were grown for additional 24–48 h prior to solubilization experiments. Hoechst nuclear dye was applied as specified by the manufacturer immediately before an experiment.

For live cell fluorescence microscopy, glass coverslips were mounted into an imaging chamber, which was filled with 150 μL of buffer solution (50 mM Tris, pH 8; 150 mM NaCl). Cells were imaged with a Nikon Ti inverted microscope (Tokyo, Japan) equipped with a Plan Fluor 40 ×/1.30 oil objective (Nikon). Imaging was controlled using the MicroManager software (Vale Lab, UCSF), which is an extension of ImageJ. Fluorescent images were taken using filters for blue (ET-EBFP2 (49021)), green (ET-GFP (49002)) or red (ET-mCherry (49008)) (Chroma Technology, Bellows Falls, VT). Additionally, cells were imaged in differential interference contrast mode. To improve reproducibility of the results, imaging areas were chosen in the center of the cover slips. Exposure times were optimized per channel and spacing between frames was set to ~3–6 s.

After acquisition of ~10 frames, 150 μL of SMA solution at twice the desired concentration in the same buffer was added to the sample chamber with a pipette and the focus was immediately readjusted manually. Imaging was then continued for 5–30 min depending on the experiment. To mimic general conditions for membrane protein solubilization by SMA, all experiments were performed at room temperature. Control experiments in buffer devoid of solubilizing agent showed no influence on cell morphology on the experimental time scale.

In membrane perforation experiments, a SMA concentration of 0.1% (w/v) was used, to be able to distinguish single steps in the process. Higher concentrations were found to accelerate the process up to the point that temporal resolution was insufficient to observe single-cell effects or step-wise perforation, whereas lower concentrations were only partially effective in inducing leakage, as seen by the presence of intact single cells even after > 20 min of incubation (see Fig. S1). For experiments with membrane protein solubilization, a higher SMA concentration of 0.33% (w/v) was chosen since solubilization was found to be generally slower than membrane perforation. Higher concentrations of SMA were avoided because they promoted detaching of cells, which strongly impaired data acquisition.

2.4. Quantification of fluorescence intensity

For quantification, images were analyzed for mean intensity per cell with the multi measure plugin in the ImageJ software. The positions of individual cells were marked using the freehand selection tool and images were analyzed per single channel. Intensities were corrected for background effects by analyzing nearby regions of approximately the same area that did not show initial fluorescence. Background-corrected data were normalized for the fluorescence intensity at the point of addition of SMA and leakage or solubilization midtimes were determined as the time at which the fluorescence intensity had dropped to 50% of the initial value. In cases where transitions were incomplete (MARCKS constructs), midpoints were approximated in this manner. For quantification of the effect of SMA on cell nuclei, the method had to be adapted since no decrease in fluorescence intensity of DNA-binding Hoechst dye was detected at the original location of the nucleus in the X/Y plane. Instead, fluorescence intensity increase in the direct vicinity of the nuclei was monitored to detect DNA release due to perforation of the nuclear membrane. To avoid distortion of the data, experimental settings were chosen such that photobleaching of the fluorophores generally did not cause a loss in fluorescence intensity of more than ~20% over the total imaging time. For data representation, images were exported from MicroManager using identical contrast settings for all images recorded in the same channel.

3. Results

3.1. SMA solubilizes cells in a step-wise process

To address general features of the overall solubilization process of cells, we first studied SMA-induced membrane perforation by investigating leakage processes of soluble proteins present in different cellular compartments. Fig. 1A shows fluorescence images of HeLa cells that were transfected to produce a cytosolic protein (GFP, top) together with a protein that is localized to the lumen of the endoplasmic reticulum (ER) (tagRFP-ER with calreticulin and KDEL signal sequence, middle). The addition of SMA, after an initial lag time, led to a fast leakage of cytosolic GFP, indicating plasma membrane perforation. This process affected single cells at a time at random positions in the observed area (see also Movie S1). Perforation of the plasma membrane coincided with a morphological change of the cell, as seen by a higher contrast of the nucleus (see arrows in DIC images in Fig. 1A bottom). For each cell, the ER probe was released only after an additional lag time (see asterisks in Fig. 1A). The differences between leakage of cytosol and ER lumen can be clearly seen from a quantitative analysis of the loss in fluorescence intensity per single cell (Fig. 1B and C, for more

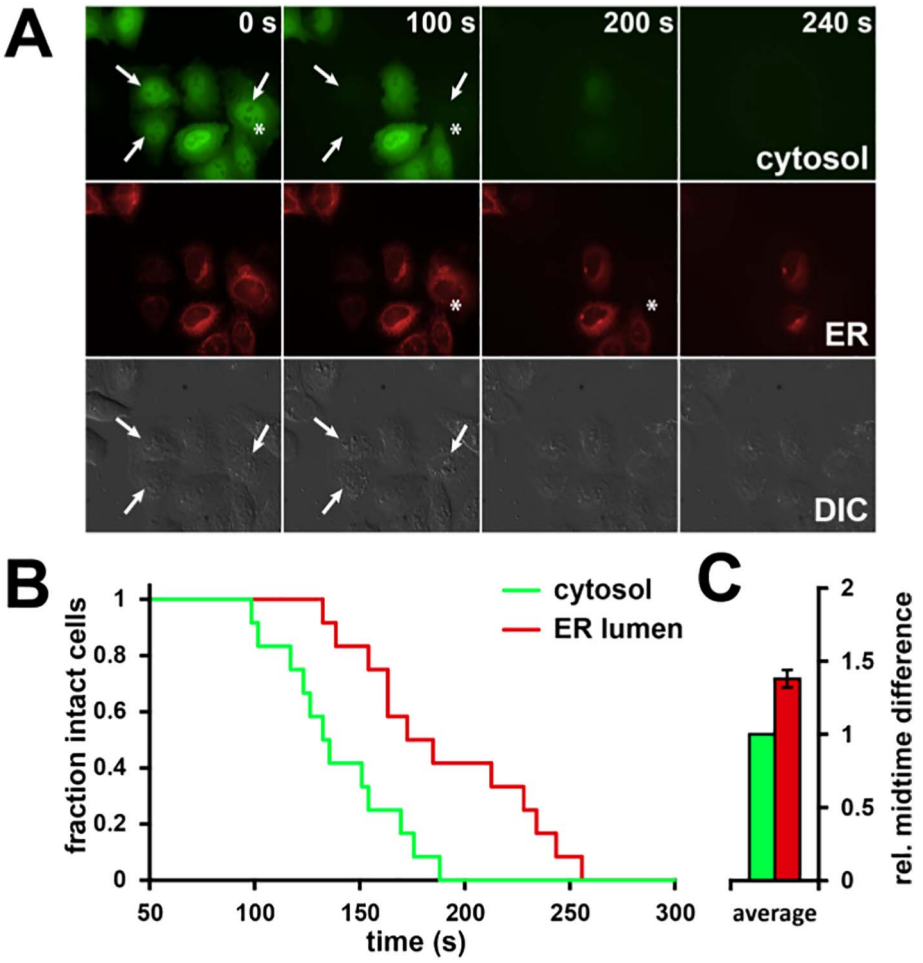

Fig. 1. Perforation of HeLa (sub)cellular membranes by SMA. (A) Top/middle: fluorescence changes of cells marked with cytosolic GFP (green) and ER luminal tagRFP-ER (red) as a function of time upon addition of 0.1% (w/v) SMA. Asterisks indicate the step-wise membrane perforation for a single cell. Bottom: micrographs recorded in differential interference contrast (DIC) showing changes in overall cell morphology. (B) Population analysis based on fluorescence decline of single cells. (C) Relative difference in leakage midtimes per cell. Data are given as averages of leakage midtimes of 12 individual cells with error bars indicating the standard deviation. Data are normalized for GFP leakage per single cell. Experiments were performed at room temperature. For details on quantification see Fig. S2.

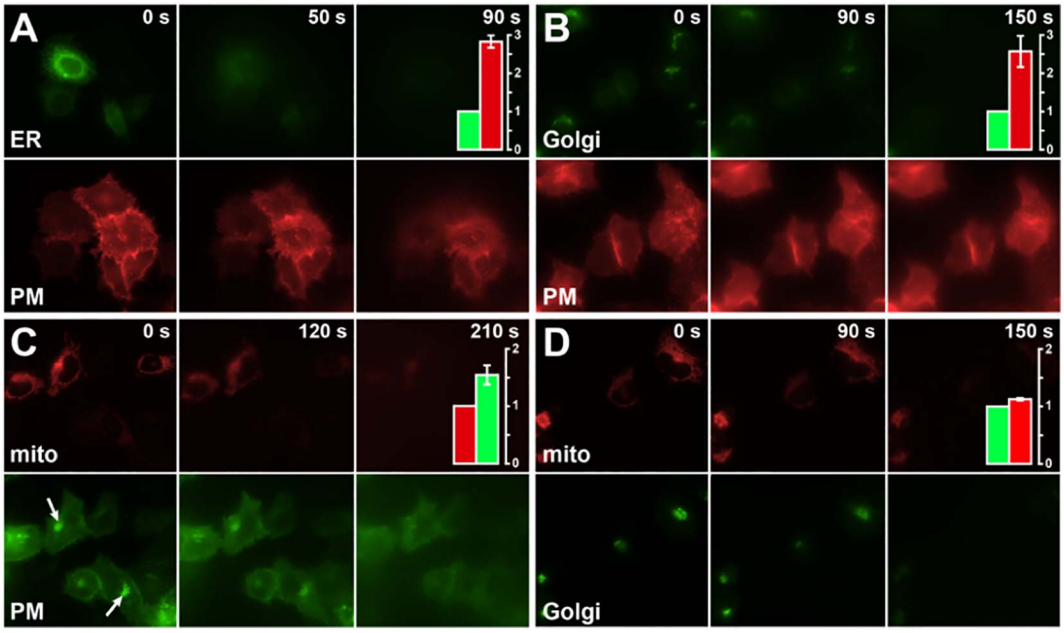

Fig. 2. Solubilization of (sub)cellular membranes by SMA. (A–C) Single-channel representations of cells expressing markers for intracellular compartments (top, A: CD8-GFP, endoplasmic reticulum; B: ManII-GFP, Golgi apparatus; C: TOM20-mCherry, outer mitochondrial membrane) together with a plasma membrane marker (MARCKS-RFP/GFP, bottom). (D) Single-channel representation for cells co-expressing markers for mitochondria (top) and Golgi (bottom). Column diagrams represent relative differences in solubilization midtimes per channel and cell (see Fig. 1C). Data are normalized for the faster solubilizing marker. Error bars are given as standard deviations of 4–10 individual cells. SMA concentration was 0.33% (w/v).

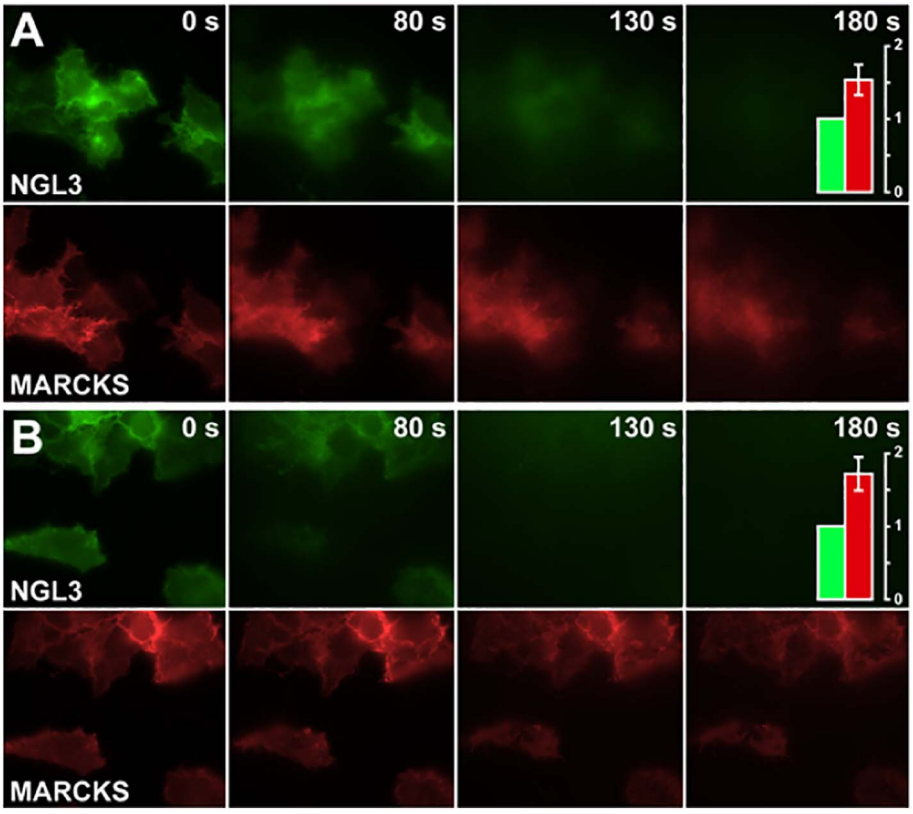

Fig. 3. Differential solubilization of different plasma membrane markers by SMA (A) and Triton X-100 (B). Solubilizing agent was added to cells containing the integral membrane protein NGL3-GFP (top, green) together with lipid-anchored MARCKS-RFP (bottom, red). Images are shown in single-channel mode over time after addition of 0.33% (w/v) solubilizing agent. Column diagram insets depict relative solubilization midtime differences analogous to Fig. 1C.

details see Fig. S2). Such a delayed leakage of the ER lumen is to be expected since SMA first needs to cross the plasma membrane before it can get access to intracellular compartments.

Interestingly, leakage midtimes varied strongly between individual cells (Fig. 1B), with the first cells being affected almost twice as fast as the last despite their close spatial proximity in the order of tens of micrometers. This hints at a high importance of local conditions, such as SMA concentration and the physical state of each individual cell. A likely explanation for the observed lag times would be a gradual accumulation of SMA on/in membranes before a threshold concentration is reached that causes membrane perforation (“all or none” effect).

Similar step-wise processes were observed in additional experiments visualizing the perforation of mitochondrial and nuclear membranes using a mitochondrial marker protein (Fig. S3) and a DNA-binding dye (Fig. S4), respectively. In all cases, organelle leakage occurred much later than cytosol leakage, supporting the generality of a step-wise process of cell solubilization by SMA.

3.2. Intracellular membranes are solubilized faster than the plasma membrane

In a further set of experiments we assessed actual solubilization of membranes by SMA, using fluorescent membrane proteins. In order to achieve efficient membrane protein solubilization, the SMA concentration was increased to 0.33% (w/v). To investigate possible preferences of SMA for specific (sub)cellular membranes, we used combinations of a lipid-anchored plasma membrane marker (MARCKS-RFP/GFP) with single-span integral membrane protein fusion constructs of complementary color that were targeted to different organelles. Upon addition of SMA, we observed a relatively fast and efficient solubilization of the markers for ER (CD8-GFP, truncated CD8 construct that is not trafficked from the ER in HeLa cells, Fig. 2A) and Golgi (ManII-GFP, Fig. 2B). In both cases, plasma membrane solubilization was much slower and some residual fluorescence could still be detected after 5 min, indicating incomplete solubilization under these conditions.

A somewhat smaller time difference was observed between markers for the plasma membrane and the outer mitochondrial membrane (TOM20-mCherry, Fig. 2C). This smaller difference may be an artefact due to the accumulation of a considerable amount of the plasma membrane marker MARCKS-GFP in the Golgi in these cells (see arrows), that could be caused by the simultaneous expression of those two constructs. As a consequence, solubilization of MARCKS-GFP appears to be faster since the Golgi signal is also taken into account. An additional experiment with the markers for Golgi and mitochondria showed that the marker proteins for both organelles indeed are solubilized similarly fast (Fig. 2D). Together, these results suggest fast and non-preferential solubilization of organelles by SMA and a generally slower solubilization of the plasma membrane.

This finding is remarkable because one would expect that the plasma membrane, since it is exposed to SMA earlier and thus perforated first, should also be solubilized faster than intracellular membranes. One possible explanation for this contrasting behavior could be that MARCKS partitions into ordered domains (“lipid rafts”) that may exist in the plasma membrane due to its high cholesterol and sphingolipid content [14,21,22]. The MARCKS construct we used is palmitoylated at a cysteine close to its myristoylated amino terminus, which could promote its partitioning into ordered domains [23–26]. Such domains might be difficult to solubilize by SMA, as suggested by a recent model membrane study on phase-separating lipid mixtures [11] that showed a distinct preference of SMA to solubilize lipids in the fluid liquid-disordered phase.

3.3. Differential kinetics of plasma membrane solubilization suggest domain preferences

To further investigate possible domain-associated solubilization preferences of SMA in the plasma membrane, we generated cells that contained the lipid-anchored MARCKS together with a plasma membrane-localized integral membrane protein (NGL3-GFP). Proteins of these two classes have been associated with different propensities for

partitioning into membrane domains, with palmitoylated peripheral membrane proteins often showing a preference for partitioning into ordered domains [23–25], whereas integral membrane proteins generally favor more fluid domains [27,28].

The experiments revealed a localization of both proteins in the plasma membrane (Fig. 3). Despite this, fluorescence intensities of the probes dropped at different rates upon addition of SMA, with NGL3 being solubilized 1.5 times faster than MARCKS (Fig. 3A, Movie S2) and the latter being incompletely solubilized after 5 min. It is tempting to speculate that the differential solubilization kinetics may be due to the presence of MARCKS and NGL3 in separate membrane domains. Such domains are likely very small with estimated diameters in the range of tens of nanometers [29,30], which makes it impossible to resolve them by standard diffraction-limited light microscopy. An influence of domain localization is further supported by the observation that using Triton X-100 instead of SMA leads to similar differences in solubilization kinetics of MARCKS and NGL3, with the latter being solubilized faster (Fig. 3B, Movie S3). For Triton, a strong preference for solubilization of disordered membrane domains has long been established by studies with both model membranes [31] and cellular membranes [21].

Finally, we compared the kinetics of solubilization of proteins in fluid environments in the plasma membrane (NGL3) and an organelle membrane (TOM20) (Fig. S5). The experiments showed, rather surprisingly, that NGL3 was solubilized at a similar rate as the mitochondrial TOM20. In view of our observation of clear lag times between the perforation of these membranes by SMA (Fig. S3), this suggests a general adverse influence of plasma membrane properties on solubilization by SMA. This may be connected to the fact that the plasma membrane is the natural barrier between a cell and its environment, which implies the necessity of a higher structural stability compared to organelle membranes.

4. Discussion

Our results suggest a hierarchical multi-step process of cell solubilization by SMA, which partially reflects a model for its mode of action based on model membrane studies [8]. Initially, polymer molecules bind to membranes until a threshold concentration is reached (lag time) and the polymer starts to insert into and subsequently perforates the plasma membrane. This causes cytosolic molecules to leak out and enables SMA to access intracellular membranes where this process is repeated. Eventually, membranes are then solubilized in the form of nanodiscs. Especially this final step seems to be strongly dependent on the properties of the target membrane as seen from our results with the plasma membrane. Here, membrane perforation occurs fast whereas solubilization of membrane proteins is relatively slow. This may in part be due to a higher stability conveyed by tight interactions of the plasma membrane with components of the cytoskeleton ("picket fence" model; see e.g. ref. [32]). Another explanation is the higher cholesterol-to-phospholipid ratio in the plasma membrane compared to organelle membranes [14]. This strongly influences plasma membrane properties since cholesterol increases the order in lipid packing and it is essential for the formation of ordered domains in the plasma membrane. Differential partitioning of proteins into such lateral domains would also explain the observed differential solubilization kinetics for different plasma membrane-localized proteins (Fig. 3), although it cannot be excluded at this point that the general properties of lipid anchored (MARCKS) and integral membrane proteins (NGL3) contribute to the observed differences in solubilization kinetics. In case lateral organization of the plasma membrane is indeed the dominant effect, our data suggest that conditions exist under which SMA could potentially be used to isolate ordered domains in the form of SMA-resistant membranes by selectively removing fluid membrane domains [11], similar as has been shown for SMA-resistant protein-rich membranes [33,34]. We speculate that under such conditions the mild solubilization of proteins by SMA may be advantageous over conventional protocols exploiting detergent resistance [21] but whether this approach is indeed beneficial remains to be addressed.

The data presented here suggest that SMA is capable of extracting integral membrane proteins from all cellular membranes including the plasma membrane, which would allow their purification and characterization with their native environment in a stable and soluble form. However, it is important to realize that there are a number of additional factors that may affect the efficiency of solubilization by SMA. These include the used cell type, the type of protein or protein-specific properties in general, such as surface charge or dimension of their membrane-embedded domain. Another important factor is the membrane environment, with protein-dense membranes with relatively low lipid content [33,34] and bilayers with a high degree of lipid order [8,9,11] being challenging for SMA. For such systems, solubilization efficiency could be increased by the addition of lipid before solubilization [1,34,35] or by elevating the temperature [8,11], respectively.

Supplementary data to this article can be found online at http://dx.doi.org/10.1016/j.bbamem.2017.08.010.

Author contributions

J.M.D., C.C.H. and J.A.K designed research, J.M.D. and M.H.C.-H. performed research, J.M.D. analyzed data, J.M.D. and J.A.K. wrote the manuscript that was edited by all authors.

Transparency document

The http://dx.doi.org/10.1016/j.bbamem.2017.08.010 associated with this article can be found, in online version.

Acknowledgements

We thank John Preston, McGill Univsersity and Eunjoon Kim, KAIST for their gift of DNA constructs and we thank Cátia Frias and Max Adrian for helpful discussions. Financial support received from the European Union via the seventh framework program (Initial Training Network "ManiFold," grant 317371) to J.M.D. and J.A.K. and from the Netherlands Organization for Scientific Research (NWO-ALW-VICI) to C.C.H. is gratefully acknowledged. M.H.C.-H. was supported by the NutsOhra Foundation (grant 1104-034), and by the Dutch Brain Foundation (Hersenstichting, grant 2012(1)-141).

References

[1] T.J. Knowles, R. Finka, C. Smith, Y.-P. Lin, T. Dafforn, M. Overduin, Membrane proteins solubilized intact in lipid containing nanoparticles bounded by styrene maleic acid copolymer, J. Am. Chem. Soc. 131 (2009) 7484–7485.
[2] J.M. Dörr, S. Scheidelaar, M.C. Koorengevel, J.J. Dominguez, M. Schäfer, C.A. van Walree, J.A. Killian, The styrene–maleic acid copolymer: a versatile tool in membrane research, Eur. Biophys. J. 45 (2016) 3–21.
[3] S. Gulati, M. Jamshad, T.J. Knowles, K.A. Morrison, R. Downing, N. Cant, R. Collins, J.B. Koenderink, R.C. Ford, M. Overduin, I.D. Kerr, T.R. Dafforn, A.J. Rothnie, Detergent-free purification of ABC (ATP-binding-cassette) transporters, Biochem. J. 461 (2014) 269–278.
[4] D.J.K. Swainsbury, S. Scheidelaar, R. van Grondelle, J.A. Killian, M.R. Jones, Bacterial reaction centers purified with styrene maleic acid copolymer retain native membrane functional properties and display enhanced stability, Angew. Chem. Int. Ed. Eng. 53 (2014) 11803–11807.
[5] J.M. Dörr, M.C. Koorengevel, M. Schäfer, A.V. Prokofyev, S. Scheidelaar, E.A.W. van der Cruijsen, T.R. Dafforn, M. Baldus, J.A. Killian, Detergent-free isolation, characterization, and functional reconstitution of a tetrameric K^+ channel: the power of native nanodiscs, Proc. Natl. Acad. Sci. U. S. A. 111 (2014) 18607–18612.
[6] I. Prabudiansyah, I. Kusters, A. Caforio, A.J. Driessen, Characterization of the annular lipid shell of the Sec translocon, Biochim. Biophys. Acta Biomembr. 1848 (2015) 2050–2056.
[7] M. Jamshad, V. Grimard, I. Idini, T.J. Knowles, M.R. Dowle, N. Schofield, P. Sridhar, Y. Lin, R. Finka, M. Wheatley, O.R.T. Thomas, R.E. Palmer, M. Overduin, C. Govaerts, J.-M. Ruysschaert, K.J. Edler, T.R. Dafforn, Structural analysis of a nanoparticle containing a lipid bilayer used for detergent-free extraction of membrane proteins, Nano Res. 8 (2014) 774–789.
[8] S. Scheidelaar, M.C. Koorengevel, J. Dominguez Pardo, J.D. Meeldijk, E. Breukink,

J.A. Killian, Molecular model for the solubilization of membranes into nanodisks by styrene maleic acid copolymers, Biophys. J. 108 (2015) 279–290.
[9] C. Vargas, R. Cuevas Arenas, E. Frotscher, S. Keller, Nanoparticle self-assembly in mixtures of phospholipids with styrene/maleic acid copolymers or fluorinated surfactants, Nanoscale 7 (2015) 20685–20696.
[10] R. Cuevas Arenas, J. Klingler, C. Vargas, S. Keller, Influence of lipid bilayer properties on nanodisc formation mediated by styrene/maleic acid copolymers, Nanoscale 8 (2016) 15016–15026.
[11] J.J. Dominguez Pardo, J.M. Dörr, A. Iyer, V. Subramaniam, J.A. Killian, Solubilization of lipids and lipid phases by the styrene–maleic acid copolymer, Eur. Biophys. J. 46 (2017) 91–101.
[12] S. Scheidelaar, M.C. Koorengevel, C.A. van Walree, J.J. Dominguez Pardo, J.M. Dörr, J.A. Killian, Effect of polymer composition and pH on the solubilization of membranes by styrene–maleic acid copolymers, Biophys. J. 111 (2016) 1974–1986.
[13] M.C. Orwick, P.J. Judge, J. Procek, L. Lindholm, A. Graziadei, A. Engel, G. Gröbner, A. Watts, Detergent-free formation and physicochemical characterization of nanosized lipid-polymer complexes: Lipodisq, Angew. Chem. Int. Ed. Eng. 51 (2012) 4653–4657.
[14] G. van Meer, D.R. Voelker, G.W. Feigenson, Membrane lipids: where they are and how they behave, Nat. Rev. Mol. Cell Biol. 9 (2008) 112–124.
[15] Z. Li, K.-I. Okamoto, Y. Hayashi, M. Sheng, The importance of dendritic mitochondria in the morphogenesis and plasticity of spines and synapses, Cell 119 (2004) 873–887.
[16] K.W. Yau, P. Schätzle, E. Tortosa, S. Pages, A. Holtmaat, L.C. Kapitein, C.C. Hoogenraad, Dendrites in vitro and in vivo contain microtubules of opposite polarity and axon formation correlates with uniform plus-end-out microtubule orientation, J. Neurosci. 36 (2016) 1071–1085.
[17] P. van Bergeijk, M. Adrian, C.C. Hoogenraad, L.C. Kapitein, Optogenetic control of organelle transport and positioning, Nature 518 (2015) 111–114.
[18] C.C. Hoogenraad, A.D. Milstein, I.M. Ethell, M. Henkemeyer, M. Sheng, GRIP1 controls dendrite morphogenesis by regulating EphB receptor trafficking, Nat. Neurosci. 8 (2005) 906–915.
[19] K.J. Zaal, C.L. Smith, R.S. Polishchuk, N. Altan, N.B. Cole, J. Ellenberg, K. Hirschberg, J.F. Presley, T.H. Roberts, E. Siggia, et al., Golgi membranes are absorbed into and reemerge from the ER during mitosis, Cell 99 (1999) 589–601.
[20] S.-K. Kwon, J. Woo, S.-Y. Kim, H. Kim, E. Kim, Trans-synaptic adhesions between netrin-G ligand-3 (NGL-3) and receptor tyrosine phosphatases LAR, protein-tyrosine phosphatase δ (PTPδ), and PTPσ via specific domains regulate excitatory synapse formation, J. Biol. Chem. 285 (2010) 13966–13978.
[21] R. Schroeder, E. London, D. Brown, Interactions between saturated acyl chains confer detergent resistance on lipids and glycosylphosphatidylinositol (GPI)-anchored proteins: GPI-anchored proteins in liposomes and cells show similar behavior, Proc. Natl. Acad. Sci. U. S. A. 91 (1994) 12130–12134.
[22] K. Simons, E. Ikonen, Functional rafts in cell membranes, Nature 387 (1997) 569–572.
[23] K.A. Melkonian, A.G. Ostermeyer, J.Z. Chen, M.G. Roth, D.A. Brown, Role of lipid modifications in targeting proteins to detergent-resistant membrane rafts, J. Biol. Chem. 274 (1999) 3910–3917.
[24] T.Y. Wang, R. Leventis, J.R. Silvius, Partitioning of lipidated peptide sequences into liquid-ordered lipid domains in model and biological membranes, Biochemistry 40 (2001) 13031–13040.
[25] J. Greaves, L.H. Chamberlain, Palmitoylation-dependent protein sorting, J. Cell Biol. 176 (2007) 249–254.
[26] M. Hundt, Y. Harada, L. de Giorgio, N. Tanimura, W. Zhang, A. Altman, Palmitoylation-dependent plasma membrane transport but lipid raft-independent signaling by linker for activation of T cells, J. Immunol. 183 (2009) 1685–1694.
[27] P. Sengupta, A. Hammond, D. Holowka, B. Baird, Structural determinants for partitioning of lipids and proteins between coexisting fluid phases in giant plasma membrane vesicles, Biochim. Biophys. Acta Biomembr. 1778 (2008) 20–32.
[28] I. Levental, M. Grzybek, K. Simons, Raft domains of variable properties and compositions in plasma membrane vesicles, Proc. Natl. Acad. Sci. U. S. A. 108 (2011) 11411–11416.
[29] C. Eggeling, C. Ringemann, R. Medda, G. Schwarzmann, K. Sandhoff, S. Polyakova, V.N. Belov, B. Hein, C. von Middendorff, A. Schönle, S.W. Hell, Direct observation of the nanoscale dynamics of membrane lipids in a living cell, Nature 457 (2009) 1159–1162.
[30] I. Levental, S.L. Veatch, The continuing mystery of lipid rafts, J. Mol. Biol. 428 (2016) 4749–4764.
[31] J. Sot, M.I. Collado, J.L.R. Arrondo, A. Alonso, F.M. Goñi, Triton X-100-resistant bilayers: effect of lipid composition and relevance to the raft phenomenon, Langmuir 18 (2002) 2828–2835.
[32] A. Kusumi, C. Nakada, K. Ritchie, K. Murase, K. Suzuki, H. Murakoshi, R.S. Kasai, J. Kondo, T. Fujiwara, Paradigm shift of the plasma membrane concept from the two-dimensional continuum fluid to the partitioned fluid: high-speed single-molecule tracking of membrane molecules, Annu. Rev. Biophys. Biomol. Struct. 34 (2005) 351–378.
[33] A.J. Bell, L.K. Frankel, T.M. Bricker, High yield non-detergent isolation of photosystem I-light-harvesting chlorophyll II membranes from spinach thylakoids, J. Biol. Chem. 290 (2015) 18429–18437.
[34] D.J.K. Swainsbury, S. Scheidelaar, N. Foster, R. van Grondelle, J. Antoinette Killian, M.R. Jones, The effectiveness of styrene-maleic acid (SMA) copolymers for solubilisation of integral membrane proteins from SMA-accessible and SMA-resistant membranes, Biochim. Biophys. Acta Biomembr. (2017), http://dx.doi.org/10.1016/j.bbamem.2017.07.011 (in press).
[35] M. Orwick-Rydmark, J.E. Lovett, A. Graziadei, L. Lindholm, M.R. Hicks, A. Watts, Detergent-free incorporation of a seven-transmembrane receptor protein into nanosized bilayer Lipodisq particles for functional and biophysical studies, Nano Lett. 12 (2012) 4687–4692.